NJC

ROYAL SOCIETY OF CHEMISTRY

PAPER

View Article Online
View Journal | View Issue

Cite this: *New J. Chem.*, 2021, 45, 12024

Well-defined surface tungstenocarbyne complex through the reaction of $[W(\equiv CtBu)(CH_2tBu)_3]$ with CeO_2: a highly stable precatalyst for NOx reduction with NH_3†

Cherif Larabi,[a] Cuirong Chen,[a] Nicolas Merle,[ab] Marc Charlin,[a] Kai C. Szeto,[a] Aimery De Mallmann,[a] Anass Benayad,[c] Karima B. Meziane,[b] Akim Kaddouri,[d] Hai P. Nguyen*[e] and Mostafa Taoufik*[a]

Received 28th April 2020,
Accepted 29th May 2021

DOI: 10.1039/d0nj02146f

rsc.li/njc

A novel well-defined precatalyst for ammonia-selective catalytic reduction of NOx (NH_3-SCR), namely, $[W(\equiv CtBu)(CH_2tBu)_3]/CeO_2$, was prepared by surface organometallic chemistry and then characterized. Due to the high dispersion of the active phase, this catalyst showed excellent activity after calcination at 500 °C, described by up to 99% conversion of NOx, high N_2 selectivity, broad operation temperature window (225–500 °C), and extremely high durability for the selective catalytic reduction of NOx with NH_3.

Introduction

Significant worldwide increase in stationary thermal power plants and mobile combustion engines has resulted in the production of large quantities of carbon dioxide and nitrogen oxides (NOx). NOx emissions contribute to ecosystem damage, serious health issues, and worsen climate change *via* the greenhouse effect, acid rains, and ozone destruction.[1] Therefore, the emission-level legislation of this pollutant has been drastically tightened.[2,3]

NOx emissions have reduced through improvements such as exhaust gas recirculation, homogeneous charge compression ignition technologies, and optimized injection systems, as well as improved air control.[4] These reducing measures can lower NOx emissions, albeit with a net increase in particulate matter (PM) amount and unburned hydrocarbons. As PM and NOx emissions are totally interdependent, a decline in the former triggers a rise in the latter, and *vice versa*. Thus, to improve the combustion engine efficiency and minimize fuel consumption, it is desirable to operate at a lean fuel mixture, which is typically the case for diesel engines.[5] Under these conditions, in addition to a complete combustion product (CO_2 and H_2O), a significant amount of NOx is produced. Therefore, exhaust gas after-treatment systems are necessary in order to meet stringent harmful-emission limits. Catalysis has seen impressive developments in the field of NOx reduction since the beginning of the eighties by the implementation of three-way catalyst systems. However, the composition of diesel exhaust brings new challenges that mobilized industries, researchers, and authorities need to conform to by creating many improvements and innovative measures. The most effective and useful method for NOx removal without compromising engine performances is the selective catalytic reduction (SCR) method assisted with reducing agents (NH_3 or hydrocarbon).[6,7] The most efficient approach is SCR using ammonia (NH_3-SCR). This process leads to high NOx conversions at fairly low temperatures and in large temperature ranges.[8] Initially, this technology is set up in power plants and industrial installations since many years; however, currently, they are extensively adopted in heavy-duty and light-duty trucks as well as locomotives and ships.

A wide range of SCR catalysts have been developed. The most commercially viable and utilized catalysts are TiO_2-supported V_2O_5 with WO_3 or MoO_3 as promotors.[9,10] Although the catalytic activity of this class of materials is acceptable, they suffer from several weaknesses such as low selectivity, narrow operating temperature range, and poor deNOx activity at low temperatures; however, the most critical is another central environmental issue—the release of deleterious and toxic VOx species.[11] Hence, alternative catalysts based on transition (W, Nb, Mo, Zr, Ta)[12] and rare-earth (Ce, Y) metals have been further developed.[13] In particular, relevant studies on new catalytic systems such as

[a] *Université Lyon 1, Institut de Chimie Lyon, CPE Lyon CNRS, UMR 5128 CP2M, PCM, 43 Bd du 11 Novembre 1918, 69616 Villeurbanne Cedex, France. E-mail: mostafa.TAOUFIK@univ-lyon1.fr*
[b] *Université de Lille, CNRS, UMR 8516 - LASIRE - Laboratoire de Spectroscopie pour les Interactions, la Réactivité et l'Environnement, F-59000 Lille, France*
[c] *Université Grenoble Alpes, CEA-LITEN, 17 rue des Martyrs, 38054 Grenoble Cedex 9, France*
[d] *Université Lyon 1 - CNRS, UMR 5256, IRCELYON, 2 Avenue Albert Einstein, F-69626 Villeurbanne, France*
[e] *Toyota Motor Europe, 1930 Zaventem, Belgium. E-mail: Hai.P.Nguyen@toyota-europe.com*

† Electronic supplementary information (ESI) available. See DOI: 10.1039/d0nj02146f

WO_3–CeO_2, Nb_2O_5–CeO_2, MnOx–WO_3–CeO_2, Cu–zeolite, and Fe–zeolite have brought important improvements in the field of NOx reduction.[13–15] Due to the oxygen buffering capacity and redox properties of ceria, it is widely used in these processes.[16] The major drawbacks of pure ceria are related to low thermal resistance and weak acidity. Hence, in order to improve these properties, new ceria-based catalysts have been developed by introducing other rare-earth or transition metal oxides such as ZrO_2, TiO_2, and their modification with WO_3, resulting in improvements in redox properties, thermal stability, and surface acidity.[13,16]

Recently, through several mechanistic studies, it has been found that the catalytic activity depends not only on the acidic and redox properties of the material,[10,17] but also on the metal–support interactions.[18] In particular, the nature of the supported tungsten species is a determining factor. The reported conventional catalysts are normally prepared by uncontrolled impregnation, resulting in different species, including isolated surface tungsten sites, W_xO_y clusters, amorphous WO_3, and $Ce_2(WO_4)_3$.[19] Indeed, all these phases are observed by any characterization technique and this can therefore complicate surface species identification and obtaining structure–activity relationships.

It has been proposed that single-site heterogeneous catalysts with a controlled coordination sphere of metals are highly effective for the selective reduction of NOx.[20] The key step is the formation of isolated, supported metal species that improve metal dispersion and increase metal–support interactions. Therefore, a powerful approach known as surface organometallic chemistry (SOMC) can be applied in order to prepare such single-site species. This methodology involves the controlled grafting of a suitable organometallic precursor onto a support, creating a firmly bonded surface-based organometallic fragment. Previous studies have shown that catalytic materials prepared through this approach can lead to enhanced activity and facilitate further mechanistic studies.[21] Moreover, great efforts have been devoted toward achieving high-performance catalysts *via* a chemical design. It is believed that the missing link for the use of catalysts in automotive applications is related to increasing the amount of nanosized and atomic-scale catalysts without impinging on their size, structure, shape, and interactions. This can be carefully monitored by SOMC.[22]

However, commercial SCR catalysts are loaded with high amounts of WO_3[23,24] for ensuring higher stability and sufficient acidity, thereby increasing the NH_3 adsorption strength that improves the activity and also the selectivity by inhibiting the oxidation of NH_3.[17] This phenomenon is also found in the case of industrial metathesis catalysts, where a high amount of metal such as tungsten (~10 wt%) is required to reach high catalytic activities, despite the fact that only a low fraction of metal sites is active.[25] Based on studies that unraveled the structure of the active species,[26–28] SOMC has led to the development of well-defined highly active catalysts that contain only a low amount of metal.[29–33] On the other hand, the use of SOMC for oxidizing support and for deNOx applications is rare. We hereby report the first example of a highly active deNOx catalyst with low metal loading prepared by the grafting of a Schrock-type tungsten complex on ceria along with its characterization.

Results and discussion

Grafting of W(≡C*t*Bu)(CH_2*t*Bu)$_3$ on ceria (CeO_{2-200}) surface by SOMC

SOMC methodology has never been investigated on a ceria support for the grafting of a tungsten complex. Prior to catalyst preparation, the ceria support (CeO_2) is characterized. The IR spectrum of ceria dehydroxylated at 200 °C shown in Fig. 1 reveal four ν(O–H) vibration bands attributable to different structures of cerium hydroxyl on the surface (terminal and bridging O–H), as reported in the literature (Fig. S1, ESI†).[34,35] The intensity of the band at 3714 cm^{-1} associated with isolated OH groups is weak and the spectrum is rather dominated by the broad signal centered at 3630 cm^{-1}, which can be attributed to bridged hydroxyl groups. In addition, a large band centered at 3527 cm^{-1} corresponds to a residual cerium oxy-hydroxide phase located within the pores.[36] To achieve the grafting and functionalization of surface hydroxides under optimum conditions, it is desirable to know their amount. Among the different quantification methods, a chemical titration using $Al(iBu)_3$, a surface reaction with a highly reactive organometallic complex, has shown to be reliable.[37] This complex quantitatively reacts in pentane with surface hydroxyl groups by releasing one equivalent of isobutane per OH (Fig. S2, ESI†). The quantification of isobutane by GC shows that CeO_{2-200} contains 0.7 mmol OH g^{-1}.

The grafting reaction of W(≡C*t*Bu)(CH_2*t*Bu)$_3$ on CeO_{2-200} is carried out in pentane at room temperature for 4 h. Elemental analysis of this material reveals the presence of 3.3 wt% W, which corresponds to ~0.18 mmol W g^{-1}. The amount of carbon is found to be 2.16 wt% (1.79 mmol C g^{-1}), which gives a C/W ratio of 9.95. Furthermore, a quantitative GC analysis of the gas released during the grafting process shows the formation of 0.38 mmol of neopentane, which is ~1.9 *t*BuCH_3 per W. This corresponds to a partial consumption of surface hydroxyls (~55% of the initial surface O–H groups). Overall, the data are consistent with the formation of bipodal surface species bearing two ligands by a protonolysis with surface hydroxyls, leading to a concomitant release of around two neopentane per grafted tungsten atom, as highlighted in Scheme 1.

The textural properties of CeO_{2-200} as well as W(≡C*t*Bu)-(CH_2*t*Bu)$_3$/CeO_{2-200} were examined by nitrogen adsorption–desorption isotherm measurements; the physisorption isotherms and pore size distribution are depicted in Fig. S3 (ESI†). As shown, the shape of these material isotherms corresponds to type V

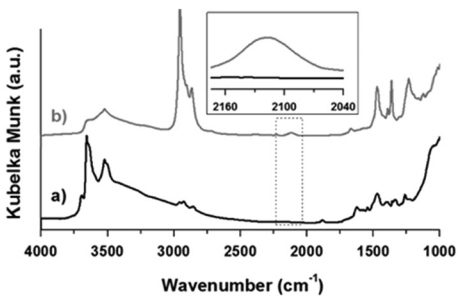

Fig. 1 DRIFT spectrum of (a) ceria dehydroxylated at 200 °C and (b) after the grafting of W(≡C*t*Bu)(CH_2*t*Bu)$_3$.

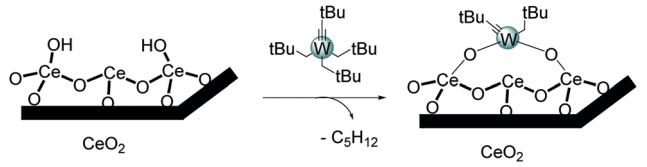

Scheme 1 Schematic illustration of the grafting of W(≡C*t*Bu)(CH_2*t*Bu)$_3$ on CeO_{2-200}.

according to IUPAC classification and shows an H2-type hysteresis loop (characteristic of capillary condensation between the aggregates constituting the solid). The initial increase in the adsorption capacity at low relative pressures is due to monolayer adsorption. The upward deviation in the range of P/P_0 = 0.5–0.7 for the support and catalyst is associated with the progressive filling of space between the aggregates of particles. The neat ceria has a specific surface area of $\sim$205 $\pm$ 10 m^2 g^{-1}. The surface area slightly decreases upon functionalization with the transition metal complex by reducing the value to 190 $\pm$ 10 m^2 g^{-1}. The pore volume also decreases from 0.24 $\pm$ 0.01 to 0.21 $\pm$ 0.01 cm^3 g^{-1}.

The grafting reaction was monitored by DRIFT spectroscopy (Fig. 1). After surface functionalization of ceria by W(≡C*t*Bu)-(CH_2*t*Bu)$_3$, the isolated ν(CeO–H) band at 3712 cm^{-1} disappeared. The new bands appearing in the ranges of 3100–2850 cm^{-1} and 1620–1400 cm^{-1} are characteristic of aliphatic ν(C–H) and δ(C–H) vibrations, respectively, of the perhydrocarbyl ligands coordinated to surface tungsten. Noteworthily, a band at 2120 cm^{-1}, which is absent in the neat ceria sample (Fig. 1a), is observed (Fig. 1b). This signal has already been found and ascribed to the forbidden $2F_{5/2}$ → $2F_{7/2}$ electronic transition of the subsurface Ce^{3+} (due to the partial reduction of ceria).[38] Moreover, the DRIFT spectrum of the resulting material (Fig. 1b) shows a partial consumption of the other OH vibration bands, located between 3700 and 3600 cm^{-1}, while a new broad band appears, resulting from the interaction of some OH groups with tungsten alkyl ligands. The evolution of signals in this spectral region with grafting has already been described for the reaction of W(≡C*t*Bu)(CH_2*t*Bu)$_3$ with alumina dehydroxylated at 500 °C, where only the terminal tetrahedral Al sites react completely.[39]

The X-ray diffraction analyses, as shown in Fig. S4 (ESI†), reveal that the samples exhibit the same diffraction peaks at 28.5°, 33.1°, 47.5°, 56.4°, 59.1°, 69.7°, and 79.1°, characteristic of the cubic fluorite structure of CeO_2.[40] This observation suggests that the functionalization did not affect the crystalline structure of ceria. From the diffraction pattern, the mean size of microcrystals can be evaluated from the Scherrer's equation. The average crystal sizes consequently estimated, as summarized in Table S1 (ESI†), indicated that the ceria particles have the tendency to agglomerate during the grafting of the tungsten complex, which corroborates the marginal reduction in the surface area.

^{1}H MAS solid-state NMR spectrum of the resulting material, as depicted in Fig. S5a (ESI†), shows large signals at −3 and 0.1 ppm, tentatively attributed to the methyl of neopentyl and neopentylidyne ligands, respectively. The ^{1}H NMR data are less informative due to the broadening and shifting of the signal positions owing to the presence of paramagnetic species (Ce^{3+}).[41,42] Moreover, from a 30% ^{13}C-labelled molecular complex, the ^{13}C CP MAS NMR data highlighted in Fig. S5b (ESI†) show an intense and broad signal centered at 26 ppm assigned to the methyl of *t*-Bu fragments and a broad—albeit weak—signal at 80 ppm, which can be assigned to the methylene carbons of the neopentyl fragment (CH_2*t*Bu). A weak signal at 287 ppm can be ambitiously attributed to the quaternary carbons of carbyne ligands. The broadening of the resonances and their shift to a higher field is presumably due to paramagnetic Ce^{3+} ions in trigonal and cubic sites present in the ceria support as already identified.[41,42]

X-ray photoelectron spectroscopy (XPS) analyses are carried out in order to provide more information on the oxidation state of the constituent elements of the sample (W, Ce, O). Fig. S6 (ESI†) shows the representative XPS spectra for Ce 3d, O 1s, and W 4f. Generally, ten features are found in the Ce 3d region due to the pairs of spin–orbit doublet, as shown in Fig. S6a and b (ESI†). Six peaks are labelled as v, v″, v‴ ($3d_{5/2}$) and u, u″, u‴ ($3d_{3/2}$), associated to Ce^{4+} and u^0, u′, v^0, v′ attributable to Ce^{3+} ($3d^{10}4f^1$), as described in the literature.[43,44] The total fraction of Ce^{3+} is estimated by taking the fitted Ce^{3+} peak areas to the total deconvoluted spectra (%Ce^{3+} = (Ce^{3+}/(Ce^{4+} + Ce^{3+}) and %Ce^{4+} = (100–%Ce^{3+}))).[45] The concentration of Ce^{3+} in the thermally treated CeO_2 is evaluated to be $\sim$32%, with respect to the total amount of Ce; therefore, the main oxidation state of ceria is Ce^{4+} (68%). Noteworthily, after the grafting of the organometallic complex, the amount of Ce^{3+} marginally increases to 34% (Table S2, ESI†), suggesting the presence of more surface oxygen vacancies.[46] It is widely reported that the concomitant presence of Ce^{3+} and Ce^{4+} offers an oxygen-buffering capacity and redox properties that can promote NOx dissociation.[47,48] The O 1s spectra of CeO_2 and W(≡C*t*Bu)-(CH_2*t*Bu)$_3$/CeO_2 are compared in Fig. S6c and d (ESI†). The peaks are quite large, leading to two binding energy contributions for O^{2-}: 531 eV and a shoulder at 532.5 eV, assigned to lattice oxygen (O^{2-}) of CeO_2 (denoted O_β)[47] and surface oxygen (denoted as O_α) such as (O^-) in the defect oxide or OH,[46] respectively. The relative amounts of calculated O_α (O_α/(O_α + O_β)) are 45% for neat CeO_2 and 37% for W(≡C*t*Bu)(CH_2*t*Bu)$_3$/CeO_{2-200}. The partial suppression of O_α can be attributed to their interaction with the grafted W.[19] The chemisorbed oxygen may promote the oxidation of NO to NO_2, inducing "fast SCR," resulting in a higher overall SCR catalytic activity.[49] Simultaneously, it can also promote the high-temperature oxidation of NH_3 and affect the selectivity.[18] Thus, an optimal amount of O_α is desirable in order to increase the reaction rate by not too much since it might affect the selectivity.[50] The XPS analysis was also used to investigate the oxidation state of tungsten loaded on the support. The W 4f signal is depicted in Fig. S6e (ESI†): it shows the presence of two signals attributable to W $4f_{5/2}$ and W $4f_{7/2}$ at 37.5 and 35.3 eV, respectively, after deconvolution. These values are characteristic of W (+VI) for the grafted complex. The W 4f peaks overlap with the Ce 5s peaks, as shown in Fig. S6f (ESI†), inducing discrepancies for curve deconvolution. Nevertheless, these results are consistent with the presence of only W (+VI), but maybe with some marginal structural heterogeneities. Electron paramagnetic resonance

Table 1 EXAFS parameters for the supported complex, W(≡C*t*Bu)-$(CH_2tBu)_3/CeO_2$. [a]The errors generated by the EXAFS fitting program "RoundMidnight" are indicated in parentheses

Type of neighbor	Number of neighbors	Distance (Å)	σ^2 (Å^2)
W≡C**C**Me$_3$	1.1(2)	1.78(1)	0.0011(6)
W-**O**Ce	1.9(3)	1.78[b]	0.0011[b]
W-**C**H$_2$CMe$_3$	1.0(2)	2.26(3)	0.0011[b]
W-**O**(Ce)	1.9(5)	2.69(2)	0.0015(10)
W-**O**(Ce)	3.0(8)	2.94(3)	0.0015[b]
W≡C**C**Me$_3$	1.1[b]	3.25(6)	0.0015[b]
W-O**Ce**	1.0(4)	3.58(3)	0.0015[b]

[a] Δk: [1.8–14.5 Å^{-1}] – ΔR: [0.5–4.0 Å]; $S_0{}^2 = 0.94$; $\Delta E_0 = 4.7 \pm 1.2$ eV (the same for all shells); fit residue: $\rho = 5.6\%$; quality factor: $(\Delta\chi)^2/\nu = 2.36$ ($\nu = 15/30$). [b] Shell constrained to a parameter above.

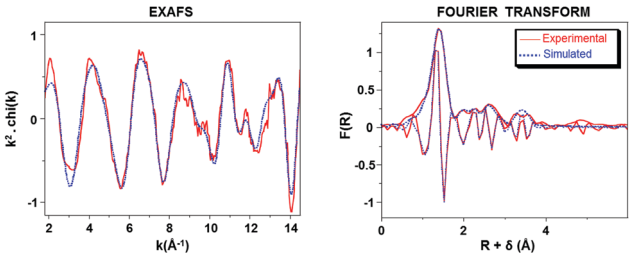

Fig. 2 W L_{III}-edge k^2-weighted EXAFS (left) and its Fourier transform (right) for W(≡C*t*Bu)$(CH_2tBu)_3/CeO_{2-200}$ material. Solid lines: experimental; dashed lines: spherical wave theory.

(EPR) spectroscopy of the W(≡C*t*Bu)$(CH_2tBu)_3/CeO_{2-200}$ material (Fig. S7, ESI†) did not show any signal of isolated W(V) ions with an expected g factor between 1.39 and 1.85.[51] This suggests that all tungsten atoms are present in the oxidation state of W(VI). The sample with 3.3 wt% W was studied by X-ray absorption spectroscopy (Table 1 and Fig. 2) in order to shed light on the structure of the supported species.

For the first peak of the Fourier transform (right in Fig. 2), two levels of coordinated light atoms back-scatterers could be evidenced at ~1.78 Å and 2.25 Å. Considering the level at 1.78 Å, two types of atoms, namely, O and C, were considered: oxygen coming from the ceria surface and carbon, from a carbyne ligand. The parameters thus extracted from the fit of the EXAFS signal are in agreement with a bipodal structure, $(-O)_2$W(≡C*t*Bu)(CH_2tBu), with around two oxygen atoms at 1.78(1) Å, around one carbon atom at 1.78(1) Å, and another carbon atom at 2.25(3) Å, attributed most probably to the carbon atoms of neopentylidyne and neopentyl ligands, respectively. The W-O distance seems marginally short but tungsten has been found to be surrounded by around six oxygen atoms at 1.787(1) Å in a $W_{0.2}Ce_{0.8}O_2$ mixed metal oxide.[52] Moreover, the two carbon back-scatterers are located at distances in the range of W≡C and W–C triple and single bonds, respectively, as observed for [W(≡C**C**Me$_3$)(=C**H**CMe$_3$)(C**H**$_2$CMe$_3$)(dmpe)] molecular complex (1.785(8) Å for W≡C*t*Bu and 2.258(9) Å for W-CH_2tBu).[53] Similar parameters were obtained when fitting the $k^3\chi(k)$ spectrum. The fit could also be improved by adding further layers of back-scatters, particularly two types of oxygen atoms at 2.69(2) and 2.94(2) Å and only around one

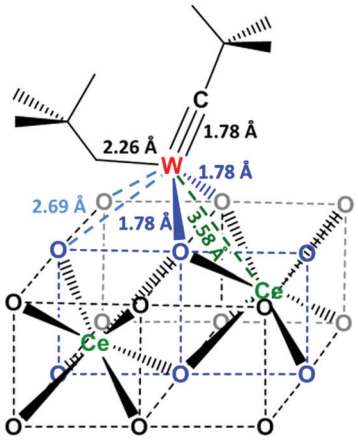

Fig. 3 Proposed structure for the species resulting from the grafting of W(≡C*t*Bu)$(CH_2tBu)_3$ onto CeO_{2-200}.

cerium atom at 3.57(3) Å. The inclusion of tungsten as a second neighbor was not statistically validated. Therefore, this EXAFS study suggests a single-site structure ($(-O)_2$W(≡C*t*Bu)-(CH_2tBu)), as shown in Fig. 3, where the tungsten atom in a pseudo-octahedral environment can be tentatively proposed (in the cerium oxide crystal,[54] the Ce–O bond distance is around 2.34 Å, and the shortest Ce–Ce distance is around 3.83 Å).

Finally, W(≡C*t*Bu)$(CH_2tBu)_3/CeO_{2-200}$ has been submitted for HRTEM study. The distribution of atomic tungsten on the surface of ceria was confirmed in an indirect manner by HRTEM and STEM analyses (Fig. S8, ESI†). Indeed, the combination of HRTEM and STEM with EDX analyses showed the homogeneity of the sample. No observable cluster or nanoparticles were observed even under extensive magnification (~1 nm), but at the same time, the EDX examination confirmed the presence of W.

The reactivity of W(≡C*t*Bu)$(CH_2tBu)_3$ with CeO_2 dehydroxylated at 200 °C has been investigated. The grafting occurs on Ce–OH groups by protonolysis, affording bipodal surface species, as suggested by the quantification of released neopentane and elemental analysis. Further characterizations by DRIFT and solid-state NMR confirm the presence of neopentyl fragments on the material. Tungsten—mainly in the oxidation state VI—has been revealed by XPS and EXAFS. XPS further provides quantitative information about the Ce^{3+}/Ce^{4+} ratio on the surface upon grafting. A more representative environment around tungsten on the surface is proposed by the EXAFS data. Surprisingly, there is only one cerium atom close to the tungsten center. The proposed model (Fig. 3) fits well with the data and comprises isolated bipodal tungsten surface species, as indicated by the elemental analysis and HRTEM.

Catalytic activity tests

The precatalyst W(≡C*t*Bu)$(CH_2tBu)_3/CeO_{2-200}$ was calcined under dry air at 500 °C for 16 h, allowing the removal of organic ligands (Fig. S9, ESI†) and affording catalyst **1** before evaluating the selective reduction of NOx in a continuous flow reactor. The temperature dependencies of NOx reduction are shown in Fig. 4. **1** shows more than 95% conversion of NOx between

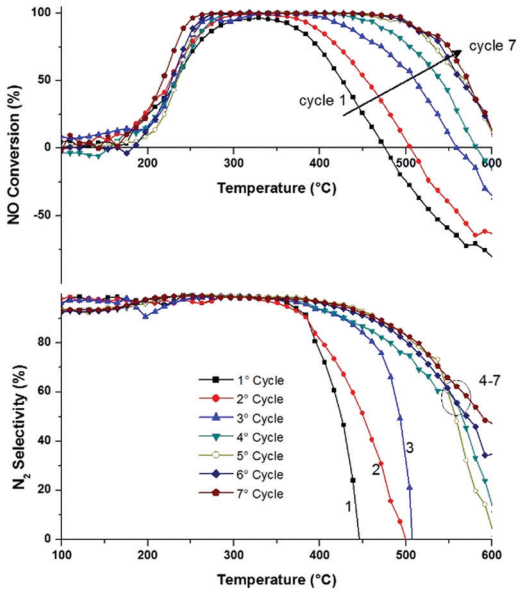

Fig. 4 NOx conversion and N_2 selectivity over **1** as a function of temperature during 7 cycles. Feed composition: 300 ppm NO, 350 ppm NH_3, and 10 vol% O_2 in He.

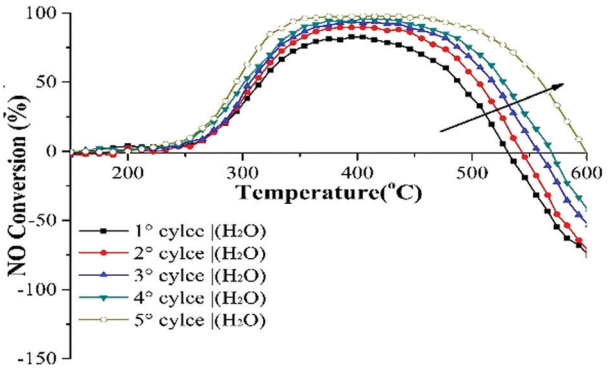

Fig. 5 NOx conversion and N_2 selectivity over **1** as a function of temperature during 5 cycles. Feed composition: 300 ppm NO, 350 ppm NH_3, 5 vol% H_2O, and 10 vol% O_2 in He.

280 and 400 °C (Fig. 4, 1st cycle). Indeed, a high activity at low temperature (200–250 °C) with a sharp increase in conversion with temperature is observed. The selectivity for N_2 is outstandingly high until 400 °C (Fig. 4). The fresh catalyst starts to oxidize NH_3 from ~400 °C, resulting in a fast drop in NO conversion and N_2 selectivity. However, upon repeating the SCR cycles, it can be observed that the same catalyst becomes more stable, selective, and temperature-resistant. Full NO conversion is maintained until 550 °C. Such evolution indicates that the surface sites responsible for NH_3 oxidation have gradually been inhibited. After five catalytic recycle tests, the catalyst seems to be stable and converts more than 99% NOx between 250 and 500 °C. This suggests that the surface species occur under the catalytic conditions (O_2, NH_3, NO, and high temperature) to achieve stable and more active species.

Moreover, the long-term stability of the catalyst at 300 °C was also studied. The results shown in Fig. S10 (ESI†) indicate that the activity of the catalysts remains stable for more than 50 h, with a conversion of about 99%. To extend the behavior of these catalysts for deNOx-related reactions, two experiments with separate (NO + O_2) and (NH_3 + O_2) feeds were performed. The results of NO and NH_3 oxidation *versus* temperature, as shown in Fig. S11 (ESI†), show that the oxidation of NO into NO_2 occurs at low temperatures, ~150 °C, and it linearly increases with the temperature to reach a pseudo-plateau between 280 and 380 °C before increasing gradually again. The first part of the curve can be explained by the role of the surface oxygen available that can promote the oxidation of NO into NO_2 to reach a plateau when oxygen is consumed. Then, thermal oxidation can follow. In contrast, the oxidation of NH_3 did not take place before the reaction temperature reaches 300 °C, where a sharp increase was observed for temperatures higher than 300 °C. This can explain the high activity observed for this SOMC catalyst (**1**), where the oxidation of NO into NO_2 is favored over NH_3 oxidation, where NO_2 can promote fast SCR.

Additional catalysis cycles have been investigated in the presence of 5% water (Fig. 5), reflecting more realistic conditions in combustion engines. Although the activity in the first cycle is far lower, which can be explained by the strong adsorption of water on the surface, the same tendency upon multiple recycling tests remains the same. After each catalytic run, the activity improves.

This better activity is due to better W dispersion on ceria, where only isolated sites are obtained in the case of the catalyst prepared *via* the SOMC approach, contrary to catalysts prepared by classical methods (**2**) composed of a statistical distribution of surface species (Fig. S12, ESI†). Therefore, the catalytic behavior is highly dependent on the preparation method. The well-controlled distribution of W species on the surface of ceria prepared through advanced surface organometallic functionalization could result in a higher concentration and strength of Brønsted acids sites[19,46] or in the formation of $W_\delta Ce_{1-\delta}O_{2-\delta}$ clusters on the surface, which are highly active and more accessible to the reactants.

Conclusions

The present work describes the first example of a deNOx catalyst prepared by SOMC. The grafting of W(≡C*t*Bu)(CH_2*t*Bu)$_3$ on CeO_2 dehydroxylated at 200 °C affords isolated bipodal species, as revealed by DRIFT, solid-state NMR, elemental analysis, TEM, XPS, and EXAFS. The catalyst transforms NO and NH_3 into N_2 in a typical exhaust gas composition after calcination at 500 °C, with almost full conversion between 280 and 400 °C. Importantly, when multiple SCR cycles were studied, the catalytic performance increased, leading to the full conversion of NO in the 220–500 °C temperature range, including that in the presence of 5 vol% water. Such an evolution is surprising, and it is presumably due to the inhibition of NH_3 oxidation by flawed sites of ceria. The good dispersion of tungsten may also increase the acidity and oxygen-buffering capacity of the material and therefore results in a more active SCR catalyst. Ongoing experiments using *in operando* techniques (EXAFS and DRIFT)

during the recycling process should provide information on the evolution of the catalyst when increasing the number of SCR cycles and explain the higher activity by the identification of different sites on the surface.

Experimental

All syntheses were performed under pure and dry argon, using standard Schlenk techniques and a glovebox. Solvents were purified and dried according to standard procedures. C_6D_6 (Aldrich, 99.8%) was distilled over Na/benzophenone and stored on NaK.

Characterization methods

Elemental analyses were performed at Mikroanalytisches Labor Pascher (Remagen, Germany). Gas-phase analyses were performed on a Hewlett Packard 5890 series II gas chromatograph equipped with a flame ionization detector and KCl/Al_2O_3 column (30 m × 0.32 mm). Diffuse reflectance infrared spectra were collected in a Nicolet 6700 FT-IR spectrophotometer at a resolution of 4 cm^{-1}. An airtight IR cell with CaF_2 windows was employed and the final spectra comprise 64 scans. Solution NMR spectra were recorded on an Avance 300 Bruker spectrometer. All chemical shifts were measured relative to residual ^1H or ^{13}C resonances in a deuterated solvent: C_6D_6, δ 7.15 ppm for ^1H, 128 ppm for ^{13}C. ^1H and ^{13}C solid-state NMR spectra were recorded on a Bruker Avance 500 spectrometer with a conventional double-resonance 4 mm CP-MAS probe. The samples were introduced under argon in a zirconia rotor (4 mm), which was then tightly closed. In all the experiments, the rotation frequency was set to 10 kHz. Chemical shifts were given with respect to tetramethylsilane (TMS) as an external reference for ^1H and ^{13}C NMR. X-ray diffraction was performed on a Siemens D8 diffractometer at Bragg–Brentano geometry (ISA, Villeurbanne). The instrument is equipped with a Cu tube (λ = 1.5406 Å). The electron paramagnetic resonance (EPR) continuous-wave (CW) measurements were performed through a sealed quartz tube on an X-band Bruker ELEXSYS E500 spectrometer operating at 9.8 GHz. The spectra were recorded with the same modulation frequency (100 kHz), the same modulation of amplitude, and the same power level for each sample. In order to avoid the saturation effect, the measurements were made at different microwave power levels (0.1–4 mW). The modulation of amplitude (1–5 G) was adjusted for the same reason. The low-temperature measurements were made with cryogenic systems. TEM measurement was executed on an environmental tomographic transmission electron microscope by FEI TITAN (IRCE Lyon, Villeurbanne). TGA was performed on a Mettler Toledo TGA2 Star^e system.

The extended X-ray absorption fine-structure (EXAFS) spectra were acquired at ELETTRA, using the XAFS beamline (experiment code: 20145422)[55] at room temperature at the tungsten L_{III}-edge. A pair of Si(111) crystals were used as the monochromator and the harmonics were rejected by the detuning of the second crystal. The spectra were recorded in the transmission mode between 9.9 and 11.43 keV. Three scans were collected for each sample. Each dataset was simultaneously collected with a W metal foil reference (11206.7 eV), and it was later aligned according to that reference (maximum in the first derivative of the first peak of the W foil). The W-supported sample was packaged within a nitrogen-filled glovebox in a double airtight sample holder equipped with Kapton windows. The data analyses were carried out using the "Athena" program and the EXAFS fitting "RoundMidnight" program, from the "MAX" package, using spherical waves. The FEFF8 program was used to calculate the theoretical files for phases and amplitudes based on model clusters of atoms. The scale factor, S_0^2 = 0.94, was evaluated from [W(≡C*t*Bu)Np_3] molecular complex diluted in BN and conditioned as a pellet (one carbon at 1.76(1) Å, with three carbon atoms at 2.10(1) Å in the first coordination sphere, and one carbon atom at 3.25(3) Å and three carbon atoms at 3.34(3) Å). The refinements were carried out by fitting the structural parameters Ni, R_i, σ_i, and energy shift, ΔE_0 (the same for all shells).

Materials

Ceria (CeO_2) HAS-5 ACTALYS 922 from Solvay ("Rare Earth La Rochelle") was calcined for 16 h at 500 °C under a flow of dry air and then evacuated under a vacuum at a high temperature. After rehydration in an inert atmosphere, ceria was partially dehydroxylated at 200 °C under a high vacuum (10^{-5} mbar) for 15 h to give a yellow solid, noted as CeO_{2-200}.

Tungsten complexes (W(≡C*t*Bu)(CH_2tBu)$_3$,[56] as well as 30% labelled W(≡*C*t*Bu)(*CH_2tBu)$_3$)[36] were prepared according to the described procedures.

Catalyst preparation: SOMC catalyst

A mixture of W(≡C*t*Bu)(CH_2tBu)$_3$ (1.6 g, 1.2 mmol) and CeO_{2-200} (7 g) was stirred in pentane (Carlo Erba, 99%) for 4 h at room temperature. The W(≡C*t*Bu)(CH_2tBu)$_3$/CeO_{2-200} material was washed three times with pentane *via* filtration–condensation cycles. Then, all the volatiles were condensed into a 6 L vessel in order to quantify neopentane evolved during the grafting reaction. After evaporation of the solvent, the resulting grey powder was dried under a vacuum (10^{-5} mbar). The material was calcined under dry air at 500 °C for 16 h before the catalytic tests.

Catalyst preparation: conventional catalyst

For comparison, the impregnated catalyst based on tungsten (W) supported on ceria was prepared by a conventional wet impregnation. In a typical reaction, at room temperature, a water-based solution of ammonium metatungstate (Aldrich, 99.99%) ($(NH_4)_6H_2W_{12}O_{40}$, 100 mg in 5 mL of water) was added to 2 g of ceria. The suspension was stirred overnight at room temperature and then water was evacuated in a rotary evaporator at 50 °C. The material obtained was then calcined under dry air at 500 °C for 16 h. The elemental analysis indicated the presence of ~3.5 wt% W.

NH_3-SCR catalytic performance tests

The NH_3-SCR catalytic evaluations were performed in a quartz fixed-bed reactor. A total gas flow rate of 300 mL min^{-1}

$$6NO + 4NH_3 \longrightarrow 5N_2 + 6H_2O$$
$$4NO + 4NH_3 + O_2 \longrightarrow 4N_2 + 6H_2O$$
$$6NO_2 + 8NH_3 \longrightarrow 7N_2 + 12H_2O$$
$$2NO_2 + 4NH_3 + O_2 \longrightarrow 3N_2 + 6H_2O$$
$$NO + NO_2 + 2NH_3 \longrightarrow 2N_2 + 3H_2O$$

Scheme 2 Reactions occurring during the SCR of NOx with NH_3.

(hourly space velocity: 30 000 h^{-1}) at atmospheric pressure, typically composed of 300 ppm NO (air liquid, crystal grade), 350 ppm NH_3 (air liquid, crystal grade), 10 vol% O_2 (air liquid, crystal grade), and 5% H_2O (when used), was sent through 30 mg of the presented catalyst diluted with 500 mg of silicon carbide in order to ensure a volume of 1 cm^3. The reactor equipped with an internal thermometer was heated from room temperature to 600 °C at a heating rate of 10 °C min^{-1}. The system was maintained at 600 °C for 10 min before cooling down. Analyses of the gas concentrations of NO, NO_2, N_2O, and NH_3 were carried out using Antaris IGS FTIR (Thermo Fisher) equipped with a gas cell of 200 mL. N_2 selectivity was evaluated assuming that the outlet gas contains no N compounds other than NO, NO_2, N_2O, and NH_3 (Scheme 2).

The catalytic activity and N_2 selectivity were calculated by the following equations:[19]

$$NO_{conversion}(\%) = \frac{[NO]_{in} - [NO]_{out} - [NO_2]_{out}}{[NO]_{in}} \times 100$$

$$N_{2selectivity}(\%) = \frac{[NH_3]_{in} + [NO]_{in} - [NO_2]_{out} - 2[N_2O]_{out} - [NH_3]_{out}}{[NH_3]_{in} + [NO]_{in}} \times 100$$

Conflicts of interest

There are no conflicts to declare.

Acknowledgements

The financial support of Toyota Motor Corporation is gratefully acknowledged. CC thanks CSC (China Scholarship Council) for financial support. At ELETTRA synchrotron light source, in Basovizza, Italy, we would like to thank Dr Luca Olivi for his help during the recording of the X-Ray absorption spectra and for the use of the glovebox.

Notes and references

1 R. M. Doherty, M. R. Heal and F. M. O'Connor, Climate change impacts on human health over Europe through its effect on air quality, *Environ. Health*, 2017, **16**, 33–44.
2 M. Fiebig, A. Wiartalla, B. Holderbaum and S. Kiesow, Particulate emissions from diesel engines: correlation between engine technology and emissions, *J. Occup. Med. Toxicol.*, 2014, **9**, 6.
3 N. Hooftman, M. Messagie, J. Van Mierlo and T. Coosemans, A review of the European passenger car regulations – Real driving emissions *vs.* local air quality, *Renewable Sustanable Energy Rev.*, 2018, **86**, 1–21.
4 S. Ramalingam, S. Rajendran and P. Ganesan, Performance improvement and exhaust emissions reduction in biodiesel operated diesel engine through the use of operating parameters and catalytic converter: a review, *Renewable Sustanable Energy Rev.*, 2018, **81**, 3215–3222.
5 F. Pischinger, The diesel engine for cars - Is there a future?, *J. Eng. Gas Turbines Power*, 1998, **120**, 641–647.
6 S. Zhang, B. Zhang, B. Liu and S. Sun, A review of Mn-containing oxide catalysts for low temperature selective catalytic reduction of NOx with NH3: reaction mechanism and catalyst deactivation, *RSC Adv.*, 2017, **7**, 26226–26242.
7 J. Xu, H. Wang, F. Guo, C. Zhang and J. Xie, Recent advances in supported molecular sieve catalysts with wide temperature range for selective catalytic reduction of NOX with C_3H_6, *RSC Adv.*, 2019, **9**, 824–838.
8 W. Shan and H. Song, Catalysts for the selective catalytic reduction of NOx with NH_3 at low temperature, *Catal. Sci. Technol.*, 2015, **5**, 4280–4288.
9 J.-K. Lai and I. E. Wachs, A Perspective on the Selective Catalytic Reduction (SCR) of NO with NH_3 by Supported V_2O_5-WO_3/TiO_2 Catalysts, *ACS Catal.*, 2018, **8**, 6537–6551.
10 G. Busca, L. Lietti, G. Ramis and F. Berti, Chemical and mechanistic aspects of the selective catalytic reduction of NOx by ammonia over oxide catalysts: a review, *Appl. Catal., B*, 1998, **18**, 1–36.
11 Z. G. Liu, N. A. Ottinger and C. M. Cremeens, Vanadium and tungsten release from V-based selective catalytic reduction diesel aftertreatment, *Atmos. Environ.*, 2015, **104**, 154–161.
12 R. Mrad, A. Aissat, R. Cousin, D. Courcot and S. Siffert, Catalysts for NOx selective catalytic reduction by hydrocarbons (HC-SCR), *Appl. Catal., A*, 2015, **504**, 542–548.
13 J. Xu, H. Yu, C. Zhang, F. Guo and J. Xie, Development of cerium-based catalysts for selective catalytic reduction of nitrogen oxides: a review, *New J. Chem.*, 2019, **43**, 3996–4007.
14 M. Moliner and A. Corma, From metal-supported oxides to well-defined metal site zeolites: the next generation of passive NOx adsorbers for low-temperature control of emissions from diesel engines, *React. Chem.*, 2019, **4**, 223–234.
15 L. Zhang, Q. Wu, X. Meng, U. Mueller, M. Feyen, D. Dai, S. Maurer, R. McGuire, A. Moini, A.-N. Parvulescu, W. Zhang, C. Shi, T. Yokoi, X. Pan, X. Bao, H. Gies, B. Marler, D. E. De Vos, U. Kolb and F.-S. Xiao, Recent advances in the preparation of zeolites for the selective catalytic reduction of NOx in diesel engines, *React. Chem. Eng.*, 2019, **4**, 975–985.
16 Z. Song, P. Liu, Y. Fu, H. Liu, Z. Huang, H. Kang, Y. Mao, B. Liu and Y. Guo, Promotional effect of acidic oxide on catalytic activity and N-2 selectivity over CeO_2 for selective catalytic reduction of NOx by NH_3, *Appl. Organomet. Chem.*, 2019, **33**, e4919.
17 G. He, Z. Lian, Y. Yu, Y. Yang, K. Liu, X. Shi, Z. Yan, W. Shan and H. He, Polymeric vanadyl species determine the

low-temperature activity of V-based catalysts for the SCR of NOx with NH_3, *Sci. Adv.*, 2018, **4**, eaau4637.

18 Z. Hu and R. T. Yang, 110th Anniversary: Recent Progress and Future Challenges in Selective Catalytic Reduction of NO by H-2 in the Presence of O-2, *Ind. Eng. Chem. Res.*, 2019, **58**, 10140–10153.

19 Y. Peng, K. Li and J. Li, Identification of the active sites on CeO_2-WO_3 catalysts for SCR of NOx with NH_3: an *in situ* IR and Raman spectroscopy study, *Appl. Catal., B*, 2013, **140**, 483–492.

20 C. Paolucci, I. Khurana, A. A. Parekh, S. Li, A. J. Shih, H. Li, J. R. Di Iorio, J. D. Albarracin-Caballero, A. Yezerets, J. T. Miller, W. N. Delgass, F. H. Ribeiro, W. F. Schneider and R. Gounder, Dynamic multinuclear sites formed by mobilized copper ions in NOx selective catalytic reduction, *Science*, 2017, **357**, 898–903.

21 N. Popoff, E. Mazoyer, J. Pelletier, R. M. Gauvin and M. Taoufik, Expanding the scope of metathesis: a survey of polyfunctional, single-site supported tungsten systems for hydrocarbon valorization, *Chem. Soc. Rev.*, 2013, **42**, 9035–9054.

22 A. Beniya and S. Higashi, Towards dense single-atom catalysts for future automotive applications, *Nat. Catal.*, 2019, **2**, 590–602.

23 F. Can, X. Courtois, S. Berland, M. Seneque, S. Royer and D. Duprez, Composition dependent performance of alumina-based oxide supported WO_3 catalysts for the NH_3-SCR reaction and the NSR plus SCR coupled process, *Catal. Today*, 2015, **257**, 41–50.

24 Y. Xu, X. Wu, L. Cao, Y. Ma, R. Ran, Z. Si, D. Weng, Z. Ma and B. Wang, Crystal orientation-dependent activity of tungsten-based catalysts for selective catalytic reduction of NOx with NH_3, *J. Catal.*, 2019, **375**, 294–303.

25 S. Lwin, Y. Li, A. I. Frenkel and I. E. Wachs, Nature of WOx Sites on SiO_2 and Their Molecular Structure–Reactivity/Selectivity Relationships for Propylene Metathesis, *ACS Catal.*, 2016, **6**, 3061–3071.

26 A. Basrur, S. Patwardhan and S. Vyas, Propene metathesis over silica-supported tungsten-oxide catalyst. Catalyst induction mechanism, *J. Catal.*, 1991, **127**, 86–95.

27 C. Martin, P. Malet, G. Solana and V. Rives, Structural analysis of silica-supported tungstates, *J. Phys. Chem. B*, 1998, **102**, 2759–2768.

28 A. Vanroomsmalen, D. Koster and J. Mol, Infrared-spectroscopy of some chemisorbed molecules on tungsten oxide-silica, *J. Phys. Chem.*, 1980, **84**, 3075–3079.

29 C. Larabi, K. C. Szeto, Y. Bouhoute, M. O. Charlin, N. Merle, A. De Mallmann, R. M. Gauvin, L. Delevoye and M. Taoufik, Solvent-Free Ring-Opening Metathesis Polymerization of Norbornene over Silica-Supported Tungsten-Oxo Perhydrocarbyl Catalysts, *Macromol. Rapid Commun.*, 2016, **37**, 1832–1836.

30 C. Larabi, N. Merle, F. Le Quemener, P. Rouge, E. Berrier, R. M. Gauvin, E. Le Roux, A. de Mallmann, K. C. Szeto and M. Taoufik, New synthetic approach towards well-defined silica supported tungsten bisoxo, active catalysts for olefin metathesis, *Catal. Commun.*, 2018, **108**, 51–54.

31 N. Merle, F. Le Quemener, Y. Bouhoute, K. C. Szeto, A. De Mallmann, S. Barman, M. K. Samantaray, L. Delevoye, R. M. Gauvin, M. Taoufik and J.-M. Basset, Well-Defined Molybdenum Oxo Alkyl Complex Supported on Silica by Surface Organometallic Chemistry: A Highly Active Olefin Metathesis Precatalyst, *J. Am. Chem. Soc.*, 2017, **139**, 2144–2147.

32 N. Merle, F. Le Quemener, S. Barman, M. K. Samantaray, K. C. Szeto, A. De Mallmann, M. Taoufik and J.-M. Basset, Well-defined silica supported bipodal molybdenum oxo alkyl complexes: a model of the active sites of industrial olefin metathesis catalysts, *Chem. Commun.*, 2017, **53**, 11338–11341.

33 F. Zhang, K. C. Szeto, M. Taoufik, L. Delevoye, R. M. Gauvin and S. L. Scott, Enhanced Metathesis Activity and Stability of Methyltrioxorhenium on a Mostly Amorphous Alumina: Role of the Local Grafting Environment, *J. Am. Chem. Soc.*, 2018, **140**, 13854–13868.

34 A. Badri, C. Binet and J. Lavalley, An FTIR study of surface ceria hydroxy groups during a redox process with H-2, *J. Chem. Soc., Faraday Trans.*, 1996, **92**, 4669–4673.

35 B. Beck, M. Harth, N. G. Hamilton, C. Carrero, J. J. Uhlrich, A. Trunschke, S. Shaikhutdinov, H. Schubert, H.-J. Freund, R. Schloegl, J. Sauer and R. Schomaecker, Partial oxidation of ethanol on vanadia catalysts on supporting oxides with different redox properties compared to propane, *J. Catal.*, 2012, **296**, 120–131.

36 M. Taoufik, E. Le Roux, J. Thivolle-Cazat, C. Coperet, J.-M. Basset, B. Maunders and G. J. Sunley, Alumina supported tungsten hydrides, new efficient catalysts for alkane metathesis, *Top. Catal.*, 2006, **40**, 65–70.

37 E. Mazoyer, J. Trebosc, A. Baudouin, O. Boyron, J. Pelletier, J.-M. Basset, M. J. Vitorino, C. P. Nicholas, R. M. Gauvin, M. Taoufik and L. Delevoye, Heteronuclear NMR Correlations To Probe the Local Structure of Catalytically Active Surface Aluminum Hydride Species on gamma-Alumina, *Angew. Chem., Int. Ed.*, 2010, **49**, 9854–9858.

38 C. Binet, A. Badri and J. Lavalley, A spectroscopic characterization of the reduction of ceria fraom electronic-transitions of intrinsic point-defects, *J. Phys. Chem.*, 1994, **98**, 6392–6398.

39 J. Joubert, F. Delbecq, P. Sautet, E. Le Roux, M. Taoufik, C. Thieuleux, F. Blanc, C. Coperet, J. Thivolle-Cazat and J.-M. Basset, Molecular understanding of alumina supported single-site catalysts by a combination of experiment and theory, *J. Am. Chem. Soc.*, 2006, **128**, 9157–9169.

40 S. A. Ansari, M. M. Khan, M. O. Ansari, S. Kalathil, J. Lee and M. H. Cho, Band gap engineering of CeO_2 nanostructure using an electrochemically active biofilm for visible light applications, *RSC Adv.*, 2014, **4**, 16782–16791.

41 R. M. Rakhmatullin, V. V. Pavlov and V. V. Semashko, EPR study of nanocrystalline CeO_2 exhibiting ferromagnetism at room temperature, *Phys. Status Solidi B*, 2016, **253**, 499–503.

42 R. M. Rakhmatullin, V. V. Semashko, S. L. Korableva, A. G. Kiiamov, A. A. Rodionov, R. Tschaggelar, J. A. van Bokhoven and C. Paun, EPR study of ceria nanoparticles containing different concentration of Ce^{3+} ions, *Mater. Chem. Phys.*, 2018, **219**, 251–257.

43 C. Anandan and P. Bera, XPS studies on the interaction of CeO_2 with silicon in magnetron sputtered CeO_2 thin films on Si and Si_3N_4 substrates, *Appl. Surf. Sci.*, 2013, **283**, 297–303.

44 Y. Zhu, N. Jain, M. K. Hudait, D. Maurya, R. Varghese and S. Priya, X-ray photoelectron spectroscopy analysis and band offset determination of CeO_2 deposited on epitaxial (100), (110), and (111)Ge, *J. Vac. Sci. Technol., B: Microelectron. Nanometer Struct.–Process., Meas., Phenom.*, 2014, **32**, 011217.

45 X. Yao, Z. Wang, S. Yu, F. Yang and L. Dong, Acid pretreatment effect on the physicochemical property and catalytic performance of CeO_2 for NH_3-SCR, *Appl. Catal., A*, 2017, **542**, 282–288.

46 W. Shan, F. Liu, H. He, X. Shi and C. Zhang, A superior Ce–W–Ti mixed oxide catalyst for the selective catalytic reduction of NOx with NH_3, *Appl. Catal., B*, 2012, **115**, 100–106.

47 X. Dong, J. Wang, H. Zhao and Y. Li, The promotion effect of CeOx on Cu-SAPO-34 catalyst for selective catalytic reduction of NOx with ammonia, *Catal. Today*, 2015, **258**, 28–34.

48 X. Yao, T. Kong, L. Chen, S. Ding, F. Yang and L. Dong, Enhanced low-temperature NH_3-SCR performance of MnOx/CeO_2 catalysts by optimal solvent effect, *Appl. Surf. Sci.*, 2017, **420**, 407–415.

49 H. Xu, M. Sun, S. Liu, Y. Li, J. Wang and Y. Chen, Effect of the calcination temperature of cerium-zirconium mixed oxides on the structure and catalytic performance of WO_3/$CeZrO_2$ monolithic catalyst for selective catalytic reduction of NOx with NH_3, *RSC Adv.*, 2017, **7**, 24177–24187.

50 S. Liu, R. Zhang, P. Li, H. Chen, Y. Wei and X. Liang, Morphology effect of diverse ceria with active tungsten species on NH_3-SCR behaviors, *Catal. Today*, 2020, **339**, 241–253.

51 S. Kuba, P. Heydorn, R. Grasselli, B. Gates, M. Che and H. Knozinger, Redox properties of tungstated zirconia catalysts: relevance to the activation of *n*-alkanes, *Phys. Chem. Chem. Phys.*, 2001, **3**, 146–154.

52 Z. Liu, W. Xu, S. Yao, A. C. Johnson-Peck, F. Zhao, P. Michorczyk, A. Kubacka, E. A. Stach, M. Fernandez-Garcia, S. D. Senanayake and J. A. Rodriguez, Superior performance of Ni–W–Ce mixed-metal oxide catalysts for ethanol steam reforming: Synergistic effects of W- and Ni-dopants, *J. Catal.*, 2015, **321**, 90–99.

53 M. Churchill and W. Youngs, Crystal-structure and molecular-geometry of W(=CCMe3)(=CHCMe3)(CH2CMe3)(DMPE), a mononuclear tungsten(VI) complex with metal-alkylidyne, metal-alkylidene, and metal-alkyl linkages, *Inorg. Chem.*, 1979, **18**, 2454–2458.

54 E. Kummerle and G. Heger, The structures of C-Ce_2O_3 + delta, Ce_7O_{12}, and $Ce_{11}O_{20}$, *J. Solid State Chem.*, 1999, **147**, 485–500.

55 A. Di Cicco and A. Filipponi, *14TH INTERNATIONAL CONFERENCE ON X-RAY ABSORPTION FINE STRUCTURE (XAFS14), PROCEEDINGS*, ed. DiCicco, A. and Filipponi, A., 2009, vol. 190.

56 D. Clark and R. Schrock, Mulitple metal-carbon bonds.12. Tungsten and molybdenum neopentylidyne and some tungsten neopentylidene complexes, *J. Am. Chem. Soc.*, 1978, **100**, 6774–6776.

